

Comparative Analysis of Experimental and Theoretical Zero-Field Splitting and Zeeman Electronic Parameters for Fe^{2+} Ions in $\text{FeX}_2 \cdot 4\text{H}_2\text{O}$ ($X = \text{F}, \text{Cl}, \text{Br}, \text{I}$) and $[\text{Fe}(\text{H}_2\text{O})_6](\text{NH}_4)_2(\text{SO}_4)_2$

M. ZAJĄC^{a,*} AND C. RUDOWICZ^{a,b}

^aInstitute of Physics (IP), West Pomeranian University of Technology, al. Piastów 17, 70-310 Szczecin, Poland

^bVisiting Professor: Faculty of Chemistry, Adam Mickiewicz University, Umultowska 89B, 61-614 Poznań, Poland

Spectroscopic and magnetic properties of Fe^{2+} ($3d^6$; $S = 2$) ions at orthorhombic sites in $\text{FeX}_2 \cdot 4\text{H}_2\text{O}$ ($X = \text{F}, \text{Cl}, \text{Br}, \text{I}$) crystals are compared with those in $[\text{Fe}(\text{H}_2\text{O})_6](\text{NH}_4)_2(\text{SO}_4)_2$ (FASH). The microscopic spin Hamiltonian modeling utilizing the package MSH/VBA enables prediction of the zero-field splitting parameters and the Zeeman electronic ones. Wide ranges of values of the microscopic parameters, i.e. the spin-orbit (λ), spin-spin (ρ) coupling constants, and the crystal-field (ligand-field) energy levels (Δ_i) within the 5D multiplet are considered to establish the dependence of the zero-field splitting parameters b_k^q (in the Stevens notation) and the Zeeman factors g_i on λ , ρ , and Δ_i . By matching the theoretical spin Hamiltonian parameters and the experimental ones measured by EMR, the suitable values of λ , ρ , and Δ_i are determined. The novel aspect is prediction of the fourth-rank zero-field splitting parameters and the ρ (spin-spin)-related contributions, not considered in previous studies. The MSH predictions provide guidance for high-magnetic field and high-frequency EMR measurements.

DOI: [10.12693/APhysPolA.132.19](https://doi.org/10.12693/APhysPolA.132.19)

PACS/topics: 33.35.+r, 71.70.Ch, 71.70.Ej, 76.20.+q, 76.30.-v, 76.30.Fc, 87.80.Lg

1. Introduction

The spin Hamiltonian (SH) parameters, including the zero-field splitting (ZFS) and the Zeeman electronic (Ze) parameters [1, 2], have recently been modeled for Fe^{2+} ions in $\text{FeX}_2 \cdot 4\text{H}_2\text{O}$ ($X = \text{F}, \text{Cl}, \text{Br}, \text{I}$) crystals, which exhibit similar crystal structure — see [3] for references. High-magnetic field and high-frequency EMR (HMF-EMR) techniques (for references, see, e.g. [4–6]) provide nowadays more reliable experimental ZFS and Ze parameter sets for $3d^4$ and $3d^6$ ($S = 2$) ions, e.g. Fe^{2+} , Mn^{3+} , and Cr^{2+} , which usually exhibit large and very large ZFS [3, 7]. Similar modeling, using the package MSH/VBA [8, 9] based on the microscopic spin Hamiltonian (MSH) approach, has recently been undertaken for $[\text{Fe}(\text{H}_2\text{O})_6](\text{NH}_4)_2(\text{SO}_4)_2$ (FASH) [10–12]. The microscopic SH (MSH) approach incorporates MSH expressions for the ZFS and Ze parameters up to fourth-order perturbation theory suitable for $3d^4$ and $3d^6$ ions with spin $S = 2$ at orthorhombic and tetragonal symmetry sites in crystals, which exhibit an orbital singlet ground state arising from the ground 5D multiplet [8, 9].

The aim of this paper is to provide a comparative analysis of experimental and theoretical ZFS and Ze parameters for Fe^{2+} ions in $\text{FeCl}_2 \cdot 4\text{H}_2\text{O}$ [3] and FASH. Pertinent theoretical background and references on the crystal-field (CF) Hamiltonian, H_{CF} and $H_{SH} = H_{Ze} + H_{ZFS}$,

which underlie this study, may be found in [3]. We note only that for both Hamiltonians we utilize the extended Stevens operators (ESO) O_k^q [13, 14]. The available data on the ground state and excited orbital states with the respective energy levels determined or adopted for Fe^{2+} ($S = 2$) ions in FASH together with the spin-orbit coupling (SOC) constants: λ_c (in crystal), λ_0 (free ion), and the orbital reduction (or covalency) factor defined as: $\lambda_c = k\lambda_0$ are surveyed to obtain input for MSH/VBA calculations. Experimental values of the ZFS parameters and energies determined for Fe^{2+} ions in FASH [10–12] are reanalyzed in view of our modeling results and compared with those obtained for Fe^{2+} ions in $\text{FeCl}_2 \cdot 4\text{H}_2\text{O}$ compounds [3]. Illustrative preliminary results for Fe^{2+} ions in FASH are presented for comparison. Detailed results and full analysis, including investigations of the role of the fourth-rank ZFS terms existing for $\tilde{S} = 2$ [1, 2], which are often omitted in experimental studies, and the spin-spin interaction contributions to the second- and fourth-rank ZFS parameters (ZFSPs) will be presented in [15].

2. $\text{FeCl}_2 \cdot 4\text{H}_2\text{O}$ vs. FASH: crystallographic, magnetic, and spectroscopic data

The structure of $\text{FeCl}_2 \cdot 4\text{H}_2\text{O}$ [16] and FASH [17] is described by the monoclinic space groups $P2_1/c$ (C_{2h}^5) and $P2_1/a$, respectively, each with two molecules in the unit cell. The unit cell is described by the lattice constants for $\text{FeCl}_2 \cdot 4\text{H}_2\text{O}$: $a = 0.5885$ nm, $b = 0.7180$ nm, $c = 0.8514$ nm, $\beta = 111.09^\circ$, $\alpha = \gamma = 90^\circ$, whereas for FASH: $a = 0.932(2)$ nm, $b = 1.265(2)$ nm, $c = 0.624(1)$ nm,

*corresponding author; e-mail: Magdalena.Zajac@zut.edu.pl

$\beta = 106.8(1)^\circ$, $\alpha = \gamma = 90^\circ$. The ionic positions of ligands around the Fe-site in the unit cell of $\text{FeCl}_2 \cdot 4\text{H}_2\text{O}$ [16] and FASH [17] indicate that the FeO_6 complex in each system represents the distorted octahedral sixfold coordination (see Fig. 1). Comparison of the structure shows that both crystals are monoclinic, however, the distances between ligands are greater for FASH, while the degree of distortions is different as evidenced by the angles: $\beta = 106.8(1)^\circ$ (FASH), $\beta = 111.09^\circ$ ($\text{FeCl}_2 \cdot 4\text{H}_2\text{O}$).

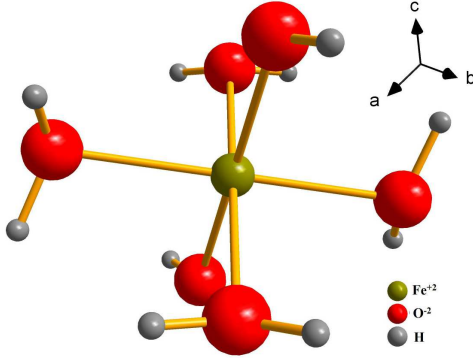


Fig. 1. The octahedral coordination of Fe^{2+} ions at orthorhombic Fe-sites in FASH (adapted from [12, 17]).

$\text{FeCl}_2 \cdot 4\text{H}_2\text{O}$ is an antiferromagnet with the Néel temperature $T_N \approx 1.1$ K [18–20], whereas the axial ZFSP $D(\text{Fe}^{2+})$ ranges as $1.25 \leq |b_2^0| \leq 2.02$ (in cm^{-1}). Experimental ZFSP values reported based on magnetic susceptibility study [18] yielded (in cm^{-1}): (i) $b_2^0 = 1.27$, $b_2^2 = -2.75$ (non-standard ZFSP set, as defined in [8, 21–23] or (ii) $b_2^0 = 2.01$, $b_2^2 = 0.53$ (standard ZFSP set). For the standardization calculations we utilize the package CST [24, 25], which is suitable for conversions, standardization, and transformations of ZFSPs (as well as the CF/LF parameters). The ZFSP values for Fe^{2+} in FASH were determined by HMF-EMR [12] as (in cm^{-1}): $|b_2^0| = 14.94(2)$ and $|b_2^2| = 11.335$. Only scant spectroscopic data are available for $\text{FeF}_2 \cdot 4\text{H}_2\text{O}$ [3, 26], which provided determination of the first few optical transitions. More relevant data exist for FASH obtained from the Mössbauer and IR spectroscopy, e.g. [10, 11, 27], as summarized in [15]. For illustration the energy levels scheme suitable for the Fe^{2+} ions in FASH [15] is shown in Fig. 2.

Using the available spectroscopic data, MSH analysis of the ZFS and Ze parameters is carried out in Sect. 3.

3. MSH modeling of the SH parameters: $\text{FeCl}_2 \cdot 4\text{H}_2\text{O}$ vs. FASH

As in Ref. [15], MSH modeling is carried out using the MSH/VBA program [8, 9] for the orthorhombic case #1 (αOI1) [28] and various sets of the microscopic input parameters: the spin-orbit (λ) and spin-spin (ρ) coupling constants, the crystal-field (ligand-field) energy levels (Δ_i) within the 5D multiplet (see Fig. 2), and s

— mixing coefficient. Since the ZFSP $b_2^0(D)$ determines major spectroscopic and magnetic features, we present comparative analysis for b_2^0 , whereas data on the ZFSP b_2^2 and the Ze parameters for $\text{FeCl}_2 \cdot 4\text{H}_2\text{O}$ and FASH may be found in the source papers [3] and [15], respectively.

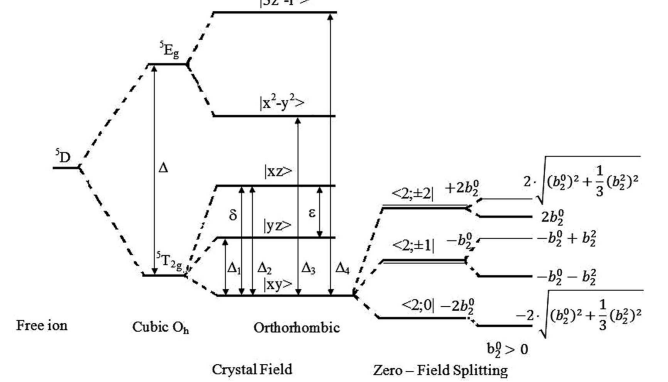


Fig. 2. Schematic energy levels for Fe^{2+} ions in FASH within the ground 5D multiplet. The energies of the excited states with respect to the ground orbital singlet are denoted in text consecutively as Δ_i , $i = 1$ to 4, whereas notation (Δ , δ , ϵ) used in [27] is also indicated.

For comparison, illustrative variations of the ZFSP b_2^0 with λ and specific values of input parameters for Fe^{2+} ions in $\text{FeCl}_2 \cdot 4\text{H}_2\text{O}$ and FASH are presented in Tables I and II, respectively. Salient features of such variations are due to the standardization procedure [8, 21–23], i.e. limiting the ratio to the standard range: $0 < E/D < 1/3$ or $0 < \lambda' = b_2^2/b_2^0 < 1$. This procedure is built-in the package MSH/VBA [8, 9] and enables automatic standardization of orthorhombic ZFSPs. This occurs for the cases when around the critical value of the variable microscopic parameter, e.g. Δ_1 or $\lambda(\text{SOC})$, $|b_2^2|$ becomes equal to $|b_2^0|$.

This equality means that $\lambda' = b_2^2/b_2^0$ reaches the threshold value of $\lambda' = 1$, at which the transition from the standard to a non-standard range (or for $\lambda' = 3$ — from one non-standard to another non-standard range [8, 21–23]) occurs. This triggers automatically the orthorhombic standardization procedure. The values approximately closest to such border points are indicated by an asterisk (*) (see Table I). The respective standardization transformations S_x , $x = 2$ to 6 are defined in [8, 21–23], whereas S1 denotes the already standard sets.

Likewise, in the graphs of the variations of the ZFSPs versus a given microscopic parameter, the standardization transitions are manifested by *apparently* discontinuous jumps as illustrated in Figs. 3 and 4 for $\text{FeCl}_2 \cdot 4\text{H}_2\text{O}$ and FASH, respectively. In general, more than one such transition may appear at specific values of a given variable quantity, e.g. $\lambda(\text{SOC})$, within the range considered. The “*apparent jumps*” in ZFSP values at the border points are indicated approximately by vertical lines (see Figs. 3 and 4). To enable visual matching the theoretic-

TABLE I

Sample variation of the ZFSPs with λ (with other input parameters fixed: $\Delta_2 = 2900$, $\Delta_3 = 8450$, $\Delta_4 = 11560$, $s = 0.00$, $\rho = 0.75$) for Fe^{2+} ions in $\text{FeCl}_2 \cdot 4\text{H}_2\text{O}$; in cm^{-1} , except the mixing coefficient s [-].

$\Delta_1 = 800$ [cm^{-1}]					
λ [cm^{-1}]	b_2^0	b_2^2	b_4^0	b_4^2	b_4^4
-60	2.47	1.37	0.06	0.12	0.20
-62	2.56	1.68	0.06	0.14	0.23
-64	2.65	2.00	0.07	0.16	0.26
-66	2.74	2.32	0.08	0.18	0.29
-68*	2.84	2.66	0.08	0.20	0.33
-70	-2.97	-2.89	0.11	0.15	0.25
-76	-3.66	-2.79	0.14	0.18	0.30
-78	-3.90	-2.76	0.16	0.19	0.32
-80	-4.14	-2.72	0.17	0.21	0.34
-90	-5.43	-2.47	0.26	0.27	0.46
-100	-6.82	-2.14	0.39	0.34	0.61
-110	-8.29	-1.72	0.55	0.43	0.81

TABLE II

Sample variation of the ZFSPs with λ (with other input parameters fixed: $\rho = 0.95$, $\Delta_3 = 10000$, $\Delta_4 = 12000$) for Fe^{2+} ions in FASH; all values in cm^{-1} .

$\Delta_1 = 300$ cm^{-1} , $\Delta_2 = 450$ cm^{-1}					
λ [cm^{-1}]	b_2^0	b_2^2	b_4^0	b_4^2	b_4^4
-110	29.74	5.95	11.00	-18.96	24.61
-100	25.57	1.35	7.57	-12.81	18.02
-90	21.20	1.51	5.01	8.27	12.90
-76	15.12	3.34	2.61	4.06	7.72
-75.5	14.91	3.37	2.54	3.95	7.57
-75	14.70	3.39	2.48	3.84	7.43
-70	12.64	3.55	1.91	2.86	6.08
-50	5.41	2.79	0.55	0.62	2.44
$\Delta_1 = 300$ cm^{-1} , $\Delta_2 = 700$ cm^{-1}					
λ [cm^{-1}]	b_2^0	b_2^2	b_4^0	b_4^2	b_4^4
-110	21.04	0.56	6.70	23.44	32.96
-100	18.21	5.27	4.60	15.79	23.38
-90	15.14	7.77	3.04	10.16	16.11
-89.5	14.99	7.85	2.97	9.92	15.80
-89	14.83	7.92	2.91	9.69	15.49
-80	12.01	8.61	1.92	6.16	10.73
-70	8.96	8.24	1.15	3.45	6.86
-68	8.37*	8.06	1.03	3.04	6.24

cal and experimental ZFSPs and facilitate determination of suitable values of λ , ρ , and Δ_i for a given system, the experimental 2nd-rank ZFSPs are represented by the horizontal lines in Figs. 3 and 4.

Finally, we consider the role of various contributions to the total ZFSPs using as an example b_2^0 and b_4^0 . The results are listed in Tables III and IV for $\text{FeCl}_2 \cdot 4\text{H}_2\text{O}$ and FASH, respectively. Since the total ZFSP values of b_2^0 and b_2^2 turn out to be non-standard range, the respective standardized (ST) values of b_2^0 and b_4^0 are also listed.

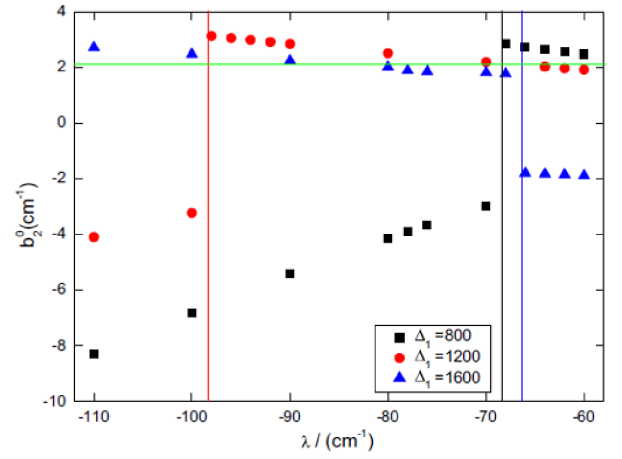


Fig. 3. The variation of the ZFSP b_2^0 versus λ for Fe^{2+} ions in $\text{FeCl}_2 \cdot 4\text{H}_2\text{O}$ for the three values of $\Delta_1 = \{800$ (black), 1200 (red), 1600 (blue) $\}$ (with other input parameters fixed: $\Delta_2 = 2900$, $\Delta_3 = 8450$, $\Delta_4 = 11560$, $s = 0.00$, $\rho = 0.75$) together with the experimental value [18]: $b_2^0 = 2.01$ (green line); all values in cm^{-1} .

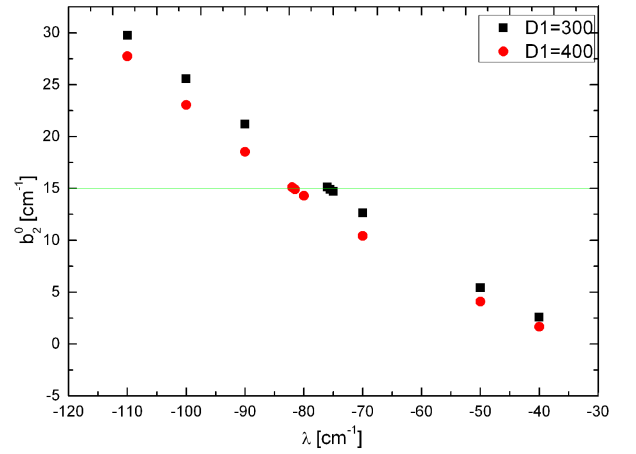


Fig. 4. The variation of the ZFSP b_2^0 versus λ for Fe^{2+} ions in FASH for the two values of $\Delta_1 (D1) = \{300$ (black), 400 (red) $\}$ (with other input parameters fixed: $\Delta_2 = 450$, $\Delta_3 = 10000$, $\Delta_4 = 12000$, $s = 0.00$, $\rho = 0.95$) together with the experimental value [12]: $b_2^0 = 15.0$ (green line); all values in cm^{-1} .

The results are listed in Tables III and IV indicate that apart from the contributions $b_2^q(\lambda^2)$, which have been only taken into account in previous studies, the contributions $b_2^q(\lambda^3)$ and $b_2^q(\rho \cdot \lambda)$ are also important. Interestingly, in some cases $b_2^0(\rho)$ may attain values larger than $b_2^0(\lambda^2)$ and of opposite sign, thus reducing the total b_2^0 , while $b_2^2(\rho) \equiv 0$ [3]. Hence, role of the ρ (spin-spin)-related contributions, as well as that of the fourth-rank ZFSPs, considered for the first time for $\text{FeCl}_2 \cdot 4\text{H}_2\text{O}$ in [3] and for FASH here, is found important. Detailed analysis of the influence of the higher-rank ZFSPs to the energy shift will be provided in [15].

TABLE III

Sample listing of the contributions to the ZFSPs (in cm^{-1}) calculated for the values of Δ_1 , λ , and ρ (with other input parameters fixed [3]), which yield close agreement with the experimental upper value of $b_2^0 \cong 2.02$ [18] for Fe^{2+} ions in $\text{FeCl}_2 \cdot 4\text{H}_2\text{O}$.

$\lambda = -70 \text{ cm}^{-1}$			$\rho = 0.75 \text{ cm}^{-1}$			
ρ [cm^{-1}]	0.55	0.75	λ [cm^{-1}]	-64	-80	
Δ_1 [cm^{-1}]	1156	1364	Δ_1 [cm^{-1}]	1200	1600	
b_2^0	ρ	-1.65	-2.25	ρ	-2.25	-2.25
	λ^2	0.64	0.32	λ^2	0.47	0.07
	λ^3	0.30	0.26	λ^3	0.22	0.34
	λ^4	-0.03	-0.02	λ^4	-0.02	-0.02
	ρ^2	0.00	0.00	ρ^2	0.00	0.00
	$\rho\lambda$	0.21	0.25	$\rho\lambda$	0.25	0.26
	total	-0.53	-1.43	total	-1.32	-1.60
	ST	2.02	2.02	ST	2.03	2.02
b_4^0	λ^4	0.02	0.01	λ^4	0.01	0.02
	ρ^2	0.00	0.00	ρ^2	0.00	0.00
	$\rho\lambda^2$	0.01	0.01	$\rho\lambda^2$	0.01	0.01
	total	0.03	0.03	total	0.02	0.03
	ST	0.04	0.04	ST	0.04	0.04

TABLE IV

Sample listing of the contributions to the ZFSPs (in cm^{-1}) calculated for the values of Δ_1 , λ , and ρ (with other input parameters fixed [15]), which yield close agreement with the experimental upper value of $b_2^0 \cong 14.942$ [12] for Fe^{2+} ions in FASH.

$\rho = 0.95$						
Δ_1 [cm^{-1}]	560	300		400		
Δ_2 [cm^{-1}]	450	450	750	450	750	
λ [cm^{-1}]	-90	-75.5	-89.5	-81.5	-95.3	
b_2^0	ρ	-2.85	-2.85	-2.85	-2.85	-2.85
	λ^2	12.99	13.38	15.31	12.87	13.69
	λ^3	6.37	6.72	6.92	6.41	6.37
	λ^4	-3.15	-4.32	-6.33	-3.35	-3.93
	ρ^2	0.00	-0.01	-0.01	-0.01	0.00
	$\rho\lambda$	1.54	1.78	1.78	1.64	1.56
	total	14.90	14.70	14.83	14.70	14.84
	ST	14.90	14.70	14.83	14.91	14.84
b_4^0	λ^4	1.76	2.31	2.82	1.94	1.96
	ρ^2	0.03	0.04	0.03	0.03	0.03
	$\rho\lambda^2$	0.13	0.14	0.05	0.14	0.10
	total	1.92	2.48	2.91	2.12	2.08
	ST	1.92	2.48	2.91	2.12	2.08

A remark on the validity of perturbation theory in the cases considered herein is pertinent. This validity hinges on the relative ratio of Δ_1 (the first excited energy level) and $\lambda(\text{SOC})$: Δ_1 should be several times larger than λ . This condition is well satisfied for Fe^{2+} ions in $\text{FeCl}_2 \cdot 4\text{H}_2\text{O}$, whereas in FASH the large values of $|b_2^0|$ for λ close to λ_0 (see Table II) indicate that the validity of perturbation theory approaches its limit. Comparison

of Figs. 3 and 4 indicate that the extent of the orbital reduction, i.e. covalency, is moderate in both compounds.

Note that generally the ZFSP sets were determined experimentally, e.g. from the magnetic susceptibility or by HMF-EMR spectroscopy for or related compounds, while neglecting the fourth-rank ZFSPs. So determined second-rank ZFSPs must be treated as approximate, since they implicitly incorporate the effects of the fourth-rank ZFSPs. It is worth mentioning that utilizing such approximation in analysis of HMF-EMR spectra would not hinder application of the $S = 2$ systems as probes for calibration of pressure during HMF-EMR measurements [4–6].

4. Conclusions

This study shows the usefulness of the MSH/VBA package [8, 9], which enables: (i) comprehensive modeling of the spin Hamiltonian parameters SHPs for $3d^4$ and $3d^6$ ($S = 2$) ions at orthorhombic and tetragonal symmetry sites, (ii) consideration of wide ranges of values of the microscopic parameters, i.e. the spin-orbit (SO: λ), spin-spin (SS: ρ) coupling constants, and the crystal-field (ligand-field) energy levels (Δ_i) within the 5D multiplet, (iii) determination of the dependence of the ZFS parameters b_k^q (in the Stevens notation) and the Zeeman factors g_i on λ , ρ , and Δ_I as well as presentation of results on suitable graphs, (iv) consideration of the role of SO (λ) and SS (ρ) coupling contributions, (v) investigations of the role of the fourth-rank ZFS terms, and (vi) comparison with DFT/*ab initio* results. By matching the theoretical predictions with the experimental (HMF-EMR, optical studies, magnetic susceptibility) data, we can achieve theoretical explanation of experimental data and determine the “best” sets of microscopic parameters.

In conclusion, the microscopic spin Hamiltonian (MSH) modeling utilizing the package MSH/VBA may provide better insight into spectroscopic and magnetic properties of $3d^4$ and $3d^6$ ($S = 2$) ions at orthorhombic and tetragonal symmetry. The data obtained due to the MSH modeling may serve for subsequent assessment of suitability of various systems as high-pressure probes for HMF-EMR [4, 6, 29].

Acknowledgments

This work was partially supported by the research grant #DEC-2012/04/M/ST3/00817 from the Polish National Science Center. The authors are grateful to Dr. P. Gnutek for helpful discussions. One of us (M.Z.) is grateful to the WPUT for a Ph.D. scholarship.

References

- [1] C. Rudowicz, M. Karbowiak, *Coord. Chem. Rev.* **287**, 28 (2015).
- [2] C. Rudowicz, S.K. Misra, *Appl. Spectrosc. Rev.* **36**, 11 (2001).

- [3] M. Zając, I.E. Lipiński, C. Rudowicz, *J. Magn. Magn. Mater.* **401**, 1068 (2016).
- [4] T. Sakurai, K. Fujimoto, R. Goto, S. Okubo, H. Ohta, Y. Uwatoko, *J. Magn. Reson.* **223**, 41 (2012).
- [5] J. Telsler, J. Krzystek, A. Ozarowski, *J. Biol. Inorg. Chem.* **19**, 297 (2014).
- [6] T. Sakurai, K. Fujimoto, R. Matsui, K. Kawasaki, S. Okubo, H. Ohta, K. Matsubayashi, Y. Uwatoko, H. Tanaka, *J. Magn. Reson.* **259**, 108 (2015).
- [7] C. Rudowicz, H.W.F. Sung, *J. Phys. Soc. Jpn.* **72**, Suppl. B, 61 (2003).
- [8] C. Rudowicz, H.W.F. Sung, *Physica B* **337**, 204 (2003).
- [9] C. Rudowicz, H.W.F. Sung, *Manual for the Package MSH/VBA*, unpublished, 2004.
- [10] J.C. Gill, P.A. Ivey, *J. Phys. C Solid State Phys.* **7**, 1536 (1974).
- [11] R. Doerfler, G.R. Allan, B.W. Davis, C.R. Pidgeon, A. Vass, *J. Phys. C Solid State Phys.* **19**, 3005 (1986).
- [12] J. Telsler, J. van Slageren, S. Vongtragool, M. Dressel, W.M. Reiff, S.A. Zvyagin, A. Ozarowski, J. Krzystek, *Magn. Reson. Chem.* **43**, S130 (2005).
- [13] C. Rudowicz, *J. Phys. C Solid State Phys.* **18**, 1415 (1985); Erratum: *ibid.* **18**, 3837 (1985).
- [14] C. Rudowicz, C.Y. Chung, *J. Phys. Condens. Matter* **16**, 5825 (2004).
- [15] M. Zając, C. Rudowicz, H. Ohta, T. Sakurai, submitted to *J. Mag. Mag. Mater.*.
- [16] J.J. Verbist, W.C. Hamilton, T.F. Koetzle, M.S. Lehmann, *J. Chem. Phys.* **56**, 3257 (1972).
- [17] H. Montgomery, R.V. Chastain, J.J. Natt, A.M. Witkowska, E.C. Lingafelter, *Acta Crystallogr.* **22**, 775 (1967).
- [18] J.T. Schriempf, S.A. Friedberg, *Phys. Rev.* **136**, A518 (1964); Erratum: *Phys. Rev. B* **2**, 781 (1970).
- [19] C.A. Raquet, S.A. Friedberg, *Phys. Rev. B* **6**, 4301 (1972).
- [20] J.N. McElearney, H. Forstat, P.T. Bailey, *Phys. Rev.* **181**, 887 (1969).
- [21] C. Rudowicz, R. Bramley, *J. Chem. Phys.* **83**, 5192 (1985).
- [22] C. Rudowicz, P. Gnutek, *Physica B* **405**, 113 (2010).
- [23] R. Kripal, D. Yadav, P. Gnutek, C. Rudowicz, *J. Phys. Chem. Solids* **70**, 827 (2009).
- [24] C. Rudowicz, in: *Crystal Field Handbook*, Eds. D.J. Newman, B. Ng, Cambridge University Press, Cambridge 2000, p. 259.
- [25] C. Rudowicz, Q. Jian, *Comp. Chem.* **26**, 149 (2002).
- [26] S. Swanepoel, *J. Phys. Chem. Solids* **50**, 935 (1989).
- [27] J.C. Gill, *J. Phys. C Solid State Phys.* **7**, 2497 (1974).
- [28] C. Rudowicz, Y.Y. Zhou, W.L. Yu, *J. Phys. Chem. Solids* **53**, 1227 (1992).
- [29] P. Gnutek, C. Rudowicz, H. Ohta, T. Sakurai, *Polyhedron* **102**, 261 (2015).